THE OHIO STATE UNIVERSITY

Building a New Galactic Synthesis Model to Aid in the Detection of Exoplanets

Research Thesis

Presented in partial fulfillment of the requirements for graduation
with research distinction in Astronomy and Astrophysics in the
College of Arts and Sciences of The Ohio State University

By

Abigail L Aronica

Thesis Committee:
Dr. Scott Gaudi, Advisor
Dr. Donald Terndrup
Samson Johnson

The Ohio State University
April 2021

ACKNOWLEDGEMENTS

I would like to thank Dr. Scott Gaudi for all of his amazing guidance, from teaching my first ever astronomy course, to his mentorship during the Summer Undergraduate Research Program, to the help he provided as I was writing this paper. I want to thank Dr. Matthew Penny for helping me to navigate my first research project and showing me that I was capable of achieving so much more than I ever thought. I thank Samson Johnson for always being there to answer my stupid questions, check in on me, and help me figure out how to be a student again in the middle of a global pandemic.

I'd also like to thank my parents, who always stood by me and supported me since I was a child painting solar system models on the walls; as well as Molly, David, and Tigist for always telling me that what I was working on sounded cool, even if they didn't completely understand what it was I was doing. Lastly, I'd like to thank all ten of my roommates, without whom I never would have made it through this final undergraduate year in one piece.

ABSTRACT

With a planned launch in 2026, one of the aims of NASA's *Nancy Grace Roman Space Telescope* (*Roman*) will perform a large survey for exoplanets by detecting gravitational microlensing events. In this work, I further developed a new Galactic population synthesis model to improve our understanding of Roman's sensitivity function. While similar Galactic models exist, there are limits on their capabilities in certain areas, particularly in modeling the Galactic bulge as well as in their ability to be adapted and modified for unique use cases. Our model aims to improve on these points and provide the *Roman* team with a concrete tool to optimize the design of the survey and better predict the number of planets that will be detected. In this paper, I will describe the methods that were used to generate the model, the outputs from the model at various parameters, and future areas of improvement for our Galactic model.

TABLE OF CONTENTS

LIST OF TABLES

LIST OF FIGURES

LIST OF ABBREVIATIONS

B | I | M | X

B

BRAVA Bulge Radial Velocity Assay.

I

IMF Initial Mass Function.

M

MIST MESA Isochrones and Stellar Tracks.

X

XHIP Extended Hipparcos Compilation.

LIST OF SYMBOLS

A | C | D | E | G | K | N | O | P | R | T | X | Z

A

ϵ : Axis ratio.

C

c : Speed of light $(2.998 * 10^8 m/s)$.

D

d_0 : Local normalization.
D_{rel} : $D_{rel}^{-1} = {D_l}^{-1} - {D_s}^{-1}$.
D_l : Distance to the lens object.
D_s : Distance to the source object.
ρ_0 : Local mass density.

E

θ_E : Radius of the Einstein Ring.
Γ : Microlensing event rate per unit time.

G

G : Gravitational constant $(6.67430 * 10^-11 \frac{Nm^2}{kg^2})$.

K

K_0 : Modified Bessell function of the second kind.

N

$n(D_l)$: Number density of lenses at distance D_l.
N_* : Number of stars.

O

τ : Optical depth.

P

μ_{rel} : Relative proper motion between the lens and source objects.

μ_b : The proper motion in galactic latitude.
μ_l : The proper motion in galactic longitude.

R

R : Galactocentric radius.
r_s : $[[(\frac{x}{x_0})^2 + (\frac{y}{y_0})^2]^2 + (\frac{z}{z_0})^4]^{1/4}$.

T

t_E : Einstein ring crossing time.

X

$\xi(m)$: $\xi(m)dm$ is the number of single stars in the mass interval m to $m + dm$.

Z

z : Height above galactic plane.

CHAPTER 1. INTRODUCTION

1.1 Microlensing

1.1.1 What is Microlensing?

When two objects pass close to each other relative to our line of sight, the gravitational field of the foreground object, also referred to as the "lens," will perturb the light from the background object, also referred to as the "source." This geometry is shown in Figure 1.1 . The magnification of the light from the source is known as a microlensing event. If the lens star has a planet around it, that planet may act as a second lens, perturbing the host star's magnification of the source to a degree that we are able to detect [1]. This method of planet detection is different from others in that it does not depend on the detection of the flux from the host star or the planet, such as with the transit method, or the gravitational influence of the planet on its host star, as with the radial velocity method [2]. Instead, we rely on the system's gravitational influence on the light coming from the source in during the microlensing event.

Planets are most easily detected using the microlensing technique when they are near the host star's Einstein ring, as shown in Figure 1.2. The radius of the Einstein ring is

$$\theta_E = \sqrt{\frac{4GM}{D_{rel}c^2}}, \tag{1.1}$$

where G is the gravitational constant, M is the mass of the lens object, c is the speed of light, and D_{rel} is a function of the distance to the source object D_s and the distance to the lens object D_l,

$$D_{rel} = ({D_l}^{-1} - {D_s}^{-1})^{-1}. \tag{1.2}$$

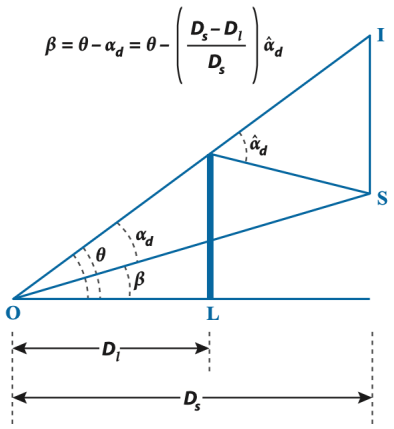

Figure 1.1. The lens (L) at a distance D_l from the observer (O) deflects light from the source (S) at distance D_s by the Einstein bending angle $\hat{\alpha}_d$. θ represents the angular position of the images, and β represents the angular position of the unlensed source. Image from Gaudi (2012) [1]

.

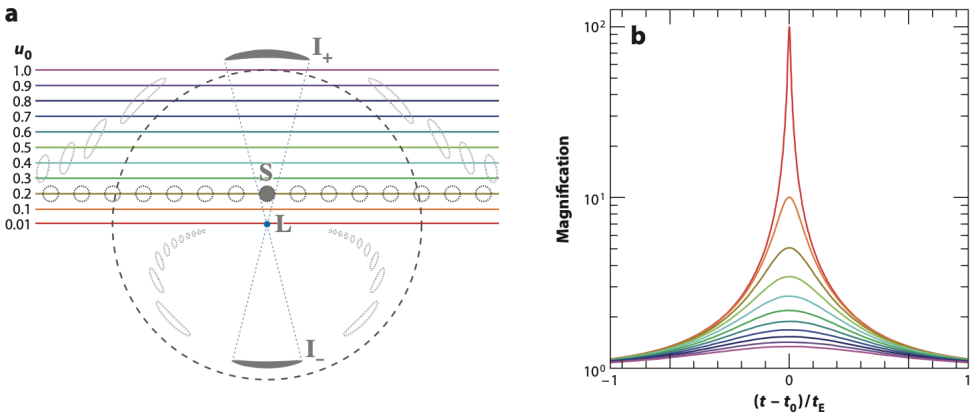

Figure 1.2. (a) The shaded circle represents the source (S), while the blue dot represents the lens (L). The gray shaded arcs show the two images of the source light that are created by the gravitational lensing. The surface brightness of the distorted images is no different from that of the original source object, so these images effectively show a magnified version of the source. The outlined circles and arcs show the source and images at various times for a trajectory with impact parameter $u_0 = 0.2$. (b) Magnification as a function of time for various impact parameters. The red line shows the closest approach to the center of the Einstein ring, while the purple line shows the furthest approach. Images from Gaudi (2012) [1]

1.1.2 What are we looking for?

In designing a microlensing survey, we want to ensure that we can detect the greatest possible number of microlensing events, and there are three important factors that one needs to consider while doing so: optical depth, timescale, and event rate.

The optical depth, also called the lensing probability, is the chance that any given source star is being gravitationally lensed by any object at a given time [3]. It can also be described as the fraction of sky covered by the Einstein rings at any given time. This can be written as

$$\tau = \int_0^{D_s} n(D_l)\pi {\theta_E}^2 {D_l}^2 dD_l \tag{1.3}$$

where $n(D_l)$ is the number density of lenses at a distance D_l. It is important to note here that the optical depth only depends on the distances of both the lens star and the source star, and does not depend on the kinematics of the system.

Next, we need to consider the timescale on which these events occur. For a single microlensing event, the time it takes for the source object to cross through the Einstein ring of the lens object is

$$t_E = \frac{\theta_E}{\mu_{rel}}, \tag{1.4}$$

where μ_{rel} is the relative proper motion between the lens star and the source star.

The other factor to consider is the microlensing event rate - the number of microlensing events that are happening per unit time for a number of source stars N_*. From Mao (2008), this value can be calculated as

$$\Gamma = \frac{d(N_*\tau)}{dt} = N_* \int_0^{D_s} n(D_l) \left(\frac{2}{\pi t_E} \pi {D_l}^2 {\theta_E}^2 \right) dD_l. \tag{1.5}$$

In order for this survey to be as successful as possible, we would like to find a location in

the Milky Way where we can maximize optical depth and event rate. Optical depth increases for source stars that are farther away, since there is more space between us and the source for a lens star to pass through. Event rate increases with the density of stars in a specific region, as there are more stars to be lensed. Therefore, the key for this study is to find a region of the Milky Way where we can see the highest density of stars (taking extinction into account).

1.2 Milky Way Structure

For the purposes of this model, the galaxy has been split into four components - the thin disk, thick disk, halo, and bulge.

The galactic bulge is the most densely populated region of the galaxy, and contains mostly older stars. We decided on a bar angle of 29.4 degrees from our line of sight, as established by Cao et al. (2013) [4], with kinematics as established by Bovy et al. (2019) [5].

The thin and thick disk of the Milky Way are distinct both chemically and kinematically, with the thick disk being older than the thin disk. The formation history of theses disks is unclear - competing theories suggest either that the two disks were formed separately, or that the thick disk is the result of stellar migration and/or flaring of stars previously located in the thin disk. Regardless, the distinctions between them make it necessary for them to be considered separately for this model [6].

Lastly, the galactic halo is a very low density region and extends out to several hundred kiloparsecs. The stars in this part of the galaxy are remnants from dwarf galaxies that collided with the Milky Way. While there is some evidence to suggest that the halo may actually be divided into an inner halo and an outer halo, with slight differences in kinematics, for the purposes of this model we will be considering the stellar halo as one structure [7].

1.3 Why We Are Doing This

There are a number of reasons why it is important to engage in a new exoplanet microlensing survey, and why a model such as the one that we have designed will be useful for scientific endeavors in this field. The incredible variety of planets in our galaxy has continued to surprise us, from the early planet discoveries that were classified as a "Hot Jupiters" [8]; to the discovery of "super-Earths" by the Kepler mission [9]; to planets orbiting pulsars [10], binary star systems [11], and stars at the very bottom of the main sequence [12].

This wide range of planets that have already been discovered indicates that there are very few physical constraints on where exoplanets can be, and therefore that there are many more interesting types to be discovered. Because the microlensing technique can detect planets anywhere from 1 AU out to free-floating planets, the Nancy Grace Roman Space Telescope has the potential to make some amazing discoveries [2, 13]. Microlensing surveys are most sensitive, however, to planets within 1-10 AU of their host stars, for a wide range of masses, which is where other planet detection techniques such as radial velocity and transit are less likely to detect lower-mass planets [14]. A plot of the theorized parameter space of the Nancy Grace Roman Space Telescope microlensing survey, formerly referred to as WFIRST, is found in Figure 1.3. Additionally, an in-depth microlensing survey would allow us to detect free-floating planets, not orbiting a host star, as these planets can act as an independent lens object [15].

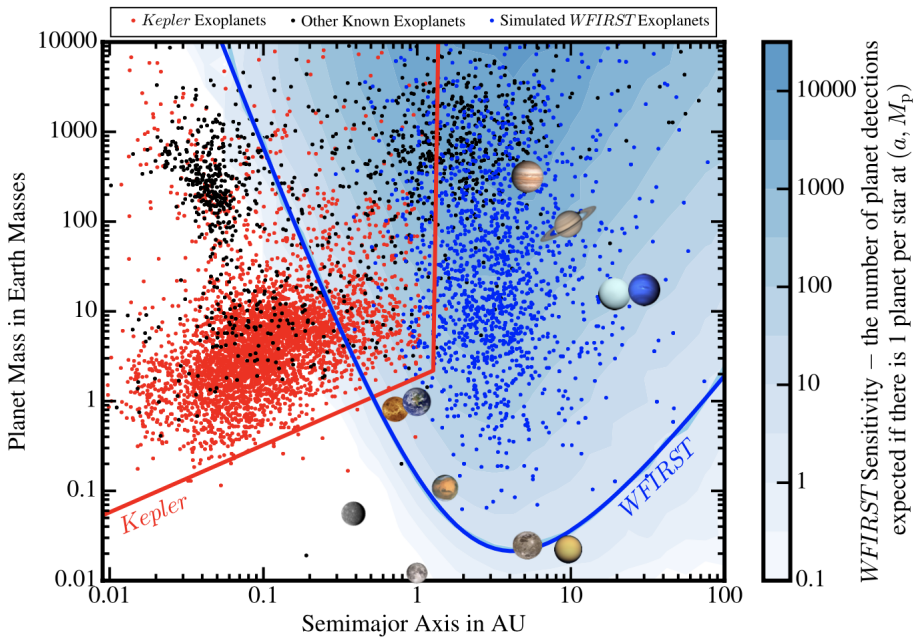

Figure 1.3. A plot showing the predictions of the Nancy Grace Roman Space Telescope (formally called WFIRST) exoplanet detections. Red dots show Kepler candidate and confirmed planets, while the solid red line shows Kepler's theoretical parameter space. Blue dots show a simulation of planets that could be detected by Roman, where the blue solid line is the theoretical parameter space for microlensing detections. Black dots show all other known planets extracted from the NASA exoplanet archive. Image from Penny (2018) [2]

1.4 Model Features

In preparation for the launch of the Nancy Grace Roman Space Telescope, we wanted to develop a computer program that would accurately model the Milky Way Galaxy, including data on stellar properties, stellar evolution, and kinematics. This would allow us to more precisely determine the locations in the galaxy where microlensing events are likely to occur the most frequently.

While there are other galactic models currently in use, including Besancon [16], TRILEGAL [17], GalMod [18], and Galaxia [19], we felt as though each of these programs lacks some of the capabilities that we desire, and that it was therefore best to design our own. At the time at which this project was started, the Besancon model lacked an accurate representation of the galactic bulge and provided little flexibility depending on the user's purposes; TRILEGAL did not include data

on kinematics, which is essential for a microlensing survey; GalMod did not include data on the mass evolution of the individual stars in the model; and Galaxia was very difficult to modify, which would have been troublesome as data on the galaxy continues to evolve.

The model that we have developed aims to incorporate aspects of previous galactic models, while improving where we feel it is necessary, in order to develop a computer program that will fit our needs. Chapter 2 of this paper will go into how this program was written, the features that it incorporates, and how it has evolved. Chapter 3 will compare the model data to observed data. Chapter 4 will address future areas of improvement for the model. Chapter 5 will conclude the paper and further discuss the importance of this project.

CHAPTER 2. BUILDING THE MODEL

A previous version of this model, constructed by Macy Huston, aimed to lay the groundwork for this project [20]. I expanded on the work that she did, and in this chapter I will explain her work as well as the additions and changes that I made.

2.1 Model Framework

The first version of this model returned a catalog of stars that would be visible according to the input parameters, which are held in a separate file that the user can edit according to their needs. The galaxy is divided into 4 distinct populations - the thin disk, thick disk, halo, and bulge [20].

2.1.1 Field of View

The user inputs parameters for the part of the galaxy that they would like to look at, and the model will output stars within this area. These parameters include a range of galactic coordinates, solid angle, and distance from the sun. This results in a conic volume of stars, extending out from the sun [20].

2.1.2 Stellar Properties

Each star is generated individually and is assigned a position, based on an equation for the stellar mass density in different areas of the galaxy as shown in Table 2.2; initial mass, as determined by the Kroupa Initial Mass Function (IMF) [21]; metallicity, as shown in Table 2.1; and set of magnitudes, according to the magnitude bands specified by the user. If the generated star is brighter than the user-specified magnitude limit in a given band, then the model goes on to calculate the velocity of the star using given circular velocity and velocity dispersion. Otherwise, the star is rejected and a new star is generated.

The Kroupa IMF is described as a multi-part power-law [21]:

$$\xi(m) \propto m^{-\alpha_i} \tag{2.1}$$

where $\xi(m)dm$ is the number of single stars in the mass interval m to $m + dm$, and

$$\begin{aligned}
\alpha_0 &= +0.3 \pm 0.7, \qquad 0.01 \leq m/M_\odot < 0.08 \\
\alpha_1 &= +1.3 \pm 0.5, \qquad 0.08 \leq m/M_\odot < 0.50 \\
\alpha_2 &= +2.3 \pm 0.3, \qquad 0.50 \leq m/M_\odot < 1.00 \\
\alpha_3 &= +2.3 \pm 0.7, \qquad 1.00 \leq m/M_\odot
\end{aligned} \tag{2.2}$$

Table 2.1 Physical Stellar Properties by Population

Population	Age (Gyr)	Metallicity	ρ_0	ϵ
Thin Disk	0-0.15	0.01 ± 0.12	$4.0 * 10^-3$	0.0140
	0.15-1	0.03 ± 0.12	$7.9 * 10^-3$	0.0268
	1-2	0.03 ± 0.10	$6.2 * 10^-3$	0.0375
	2-3	0.01 ± 0.11	$4.0 * 10^-3$	0.0551
	3-5	-0.07 ± 0.18	$5.8 * 10^-3$	0.0696
	5-7	-0.14 ± 0.17	$4.9 * 10^-3$	0.0785
	7-10	-0.37 ± 0.20	$6.6 * 10^-3$	0.0791
Thick disk	11	-0.78 ± 0.30	$1.34 * 10^-3$	
Halo	14	-1.78 ± 0.50	$9.32 * 10^-6$	0.76
Bulge	10	-0.31 ± 0.31	13.26	

Stellar properties that are necessary for this model. ρ_0 is the local mass density, and ϵ is the axis ratio. Data from Robin et al (2003) [16] and Gonzalez et al. (2015) [22].

Table 2.2 Stellar Mass Distributions

Population	Function	Constants	Limits
Thin Disk	$\frac{\rho_0}{d_0} * [exp(-(\frac{a}{h_{R+}})^2) - exp(-(\frac{a}{h_{R-}})^2)]$	$h_{R+} = 5000pc$ $h_{R-} = 3000pc$	age $\leq$ 0.15 Gyr
	$\frac{\rho_0}{d_0} * [exp(-(0.5^2 + \frac{a^2}{h_{R+}^2})^{1/2})$ $-exp(-(0.5^2 + \frac{a^2}{h_{R-}^2})^{1/2})]$	$h_{R+} = 2530pc$ $h_{R-} = 1320pc$	age $>$ 0.15 Gyr
Thick Disk	$\frac{\rho_0}{d_0} * exp(-\frac{R - R_\odot}{h_R}) * (1 - \frac{1/h_z}{x_l * (2 + x_l/h_z)} * z^2)$	$h_R = 2500pc$ $h_z = 800pc$ $x_l = 400pc$	$\lvert z\rvert \leq x_l$
	$\frac{\rho_0}{d_0} * exp(-\frac{R - R_\odot}{h_R}) * \frac{exp(x_l/h_z)}{1 + x_l/2h_z} * exp(-\frac{\lvert z\rvert}{h_z})$	$h_R = 2500pc$ $h_z = 800pc$ $x_l = 400pc$	$\lvert z\rvert > x_l$
Halo	$\frac{\rho_0}{d_0} * (\frac{a_c}{R_\odot})^{-2.44}$	$a_c = 500pc$	$a \leq a_c$
	$\frac{\rho_0}{d_0} * (\frac{a}{R_\odot})^{-2.44}$		$a > a_c$
Bulge	$\rho_0 * K_0(r_s)$[1]		

Stellar mass distributions for each population (thin disk, thick disk, halo, and bulge). d_0 is the local mass normalization, $a^2 = R^2 + \frac{z^2}{\epsilon^2}$, where R is the galactocentric radius, and z is the height above the galactic plane. Adapted from Robin et al. (2003) [16].

[1] In the case of the bulge, ρ_0 is the central density rather than local, K_0 is the modified Bessell function of the second kind, and $r_s = [[(\frac{x}{x_0})^2 + (\frac{y}{y_0})^2]^2 + (\frac{z}{z_0})^4]^{1/4}$

2.1.3 Stellar Evolution

In evolving a star to its current properties, data from the MESA Isochrones and Stellar Tracks (MIST) were used. This data provides a grid of stars with information on each, including its metallicity, age, initial mass, and luminosity. When the model generates a star, a 3-dimensional

interpolation function is used to find the point on the isochrones that most closely corresponds to that star. This is then used to determine the evolved properties of the star, such as the mass and magnitude. The model will either use a cubic interpolation function when the star is positioned consistently between data points [23], or a linear interpolation function otherwise. If a star does not fit within the parameters of the isochrones, it is assigned properties based on the closest-fitting track [20].

2.1.4 Kinematics

For this model, a solid body rotation of 45 km/s/mpc was selected to represent the inner galaxy. Once this value reaches 220 km/s, the value is then treated as a constant circular velocity. All velocity dispersions were modeled after the Besancon Model, as outlined by Robin et al. (2003) [16].

2.1.5 Extinction

There was no extinction model incorporated into the first version of this program. Users could input a constant value for extinction, but were encouraged to apply their own extinction law to the model output afterwards [20]. The addition of extinction into our model is currently in progress.

2.1.6 Galactic Components

The inaccuracies in the galactic bulge from other galactic synthesis models were one of the primary reasons that we decided to build a new model, so this area was one of the main focuses of this project. The bulge was represented by an E3 boxy-shaped bulge, as shown by Cao et al. (2013) [4]. The metallicity distribution was pulled from Gonzalez et al. (2015) [22] and can be found in Table 2.1.

The galactic disk and halo were kept consistent with that of the Besancon Model [16], with all properties shown in Table 2.1 and distribution functions shown in Table 2.2.

2.2 Recent Updates

Following this early version of the model, there were some updates that needed to be made to improve efficiency and accuracy of the program.

The first version of this program was written using Python 2, which has since been updated. It also was not written in an object-oriented format, which made running the program more cumbersome. Early updates to this model included a shift to Python 3, reorganization to an object-oriented format, and syntatical and organizational changes to keep the model up to date with Python programming standards and to ensure that it was easy to read and use by someone who does not have a background in programming.

The next task was to make changes to the program that would result in a lower computational cost and a faster runtime. One of the ways in which this was done was by importing data from the isochrones to the model using a Pandas database, as opposed to built-in data storage methods such as dictionaries. Another edit that was made in an effort to increase efficiency was to calculate the location of maximum density (for the purpose of assigning a position to a given star) using a Nelder Mead function [24]. While the SciPy library contains a minimizer function that utilizes a Nelder Mead algorithm, we found that a homemade version of the minimizer had a shorter runtime and was more easily adapted to our purposes.This function works by creating an n-pointed shape and continually moving the point with the highest value to a place of lower value until the shape converges on a single, local minimum [24]. Inverting this algorithm allows us to find the maximum value of a function, which was what we needed for this model.

CHAPTER 3. COMPARISON TO OBSERVATIONS

Comparing our model outputs to galaxy observations allows us to evaluate where our program accurately models galactic components, and where there is room for improvement.

3.1 Hertzprung-Russell Diagram

In order to evaluate stellar mass distributions, initial mass functions, and evolution in comparison with observed data, we generated a color-magnitude diagram plotting color against brightness in the I band with data from the Extended Hipparcos Compilation (XHIP) by Anderson et. al. (2012) covering the whole sky [25]. Model points were generated at $b = 0°$ and $|l| < 10°$ in order to cover a diverse population of stars in the galaxy.

One notable feature is the population of source stars at very high magnitudes, which do not seem to fit in with the observed data. While this is a small number of stars, this deviation from the expected distribution is worth investigating. It is likely that this resulted from issues in the isochrone interpolation, and that the evolved properties of the stars are being miscalculated resulting in higher than expected brightness for a very limited number of stars.

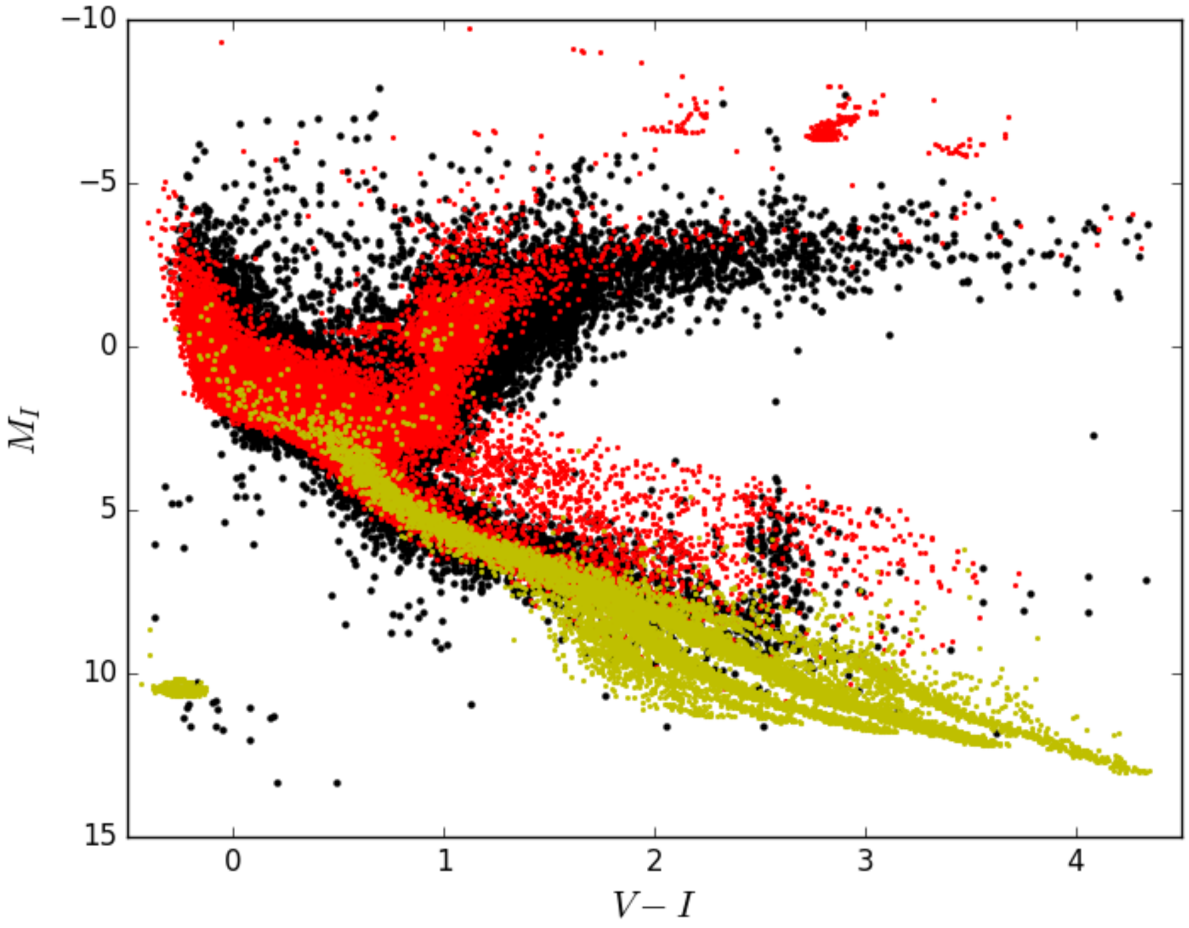

Figure 3.1. A Hertzprung-Russel diagram showing magnitude in I band as a function of color (V-I). Model sources (K ¡ 18) are shown in red, model lenses are shown in yellow, and XHIP data is shown in black. Adapted from Huston (2018) [20].

3.2 Kinematics

3.2.1 Radial Velocity

We compared model outputs with data from the Bulge Radial Velocity Assay (BRAVA) from Kunder et al. 2011 [26] to see how accurately our model simulates the kinematics of the galactic bulge, as shown in Figure 3.2.

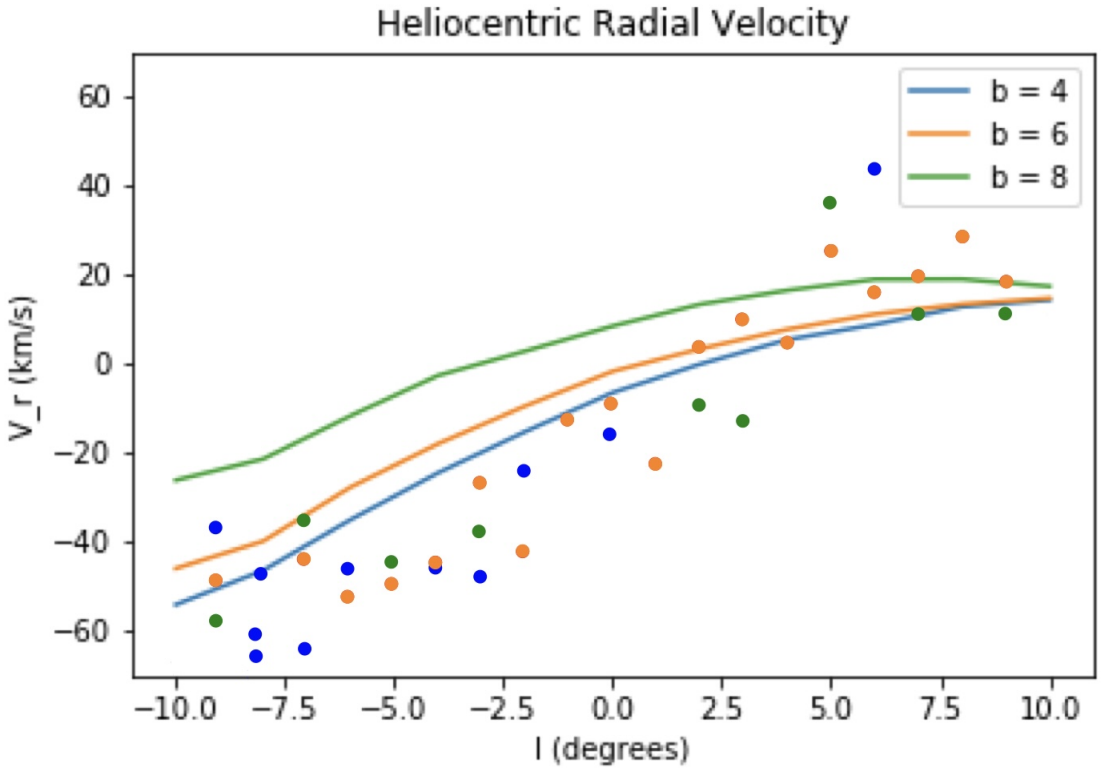

Figure 3.2. The mean radial velocity as a function of galactic longitude (l) for a selection of galactic latitudes (b).

As we can see, the model fairly accurately predicts the radial velocities, particularly at higher l, with some problems with the overestimation of the radial velocity at lower l.

3.2.2 Proper Motion

We chose to also look at the proper motions in both l and b for a selection of both bulge and disk stars at the coordinates $l = 1.25°, b = -2.65°$, which was similarly analyzed by Clarkson et al. (2008) [27]. Shown in Figure 3.3 is the model data, while shown in Figure 3.4 is the Clarkson et al. data.

We first notice that the distributions of μ_l from the model are skewed to the right relative to the data from Clarkson et al., which is something that should be further looked into. However, the heights and widths of the two peaks relative to each other are similar to that of the observed data.

The distirbutions of μ_b are very similar from our model to that of Clarkson et al., though skewed slightly to the right. This is likely a similar issue as with μ_l, and should be investigated further.

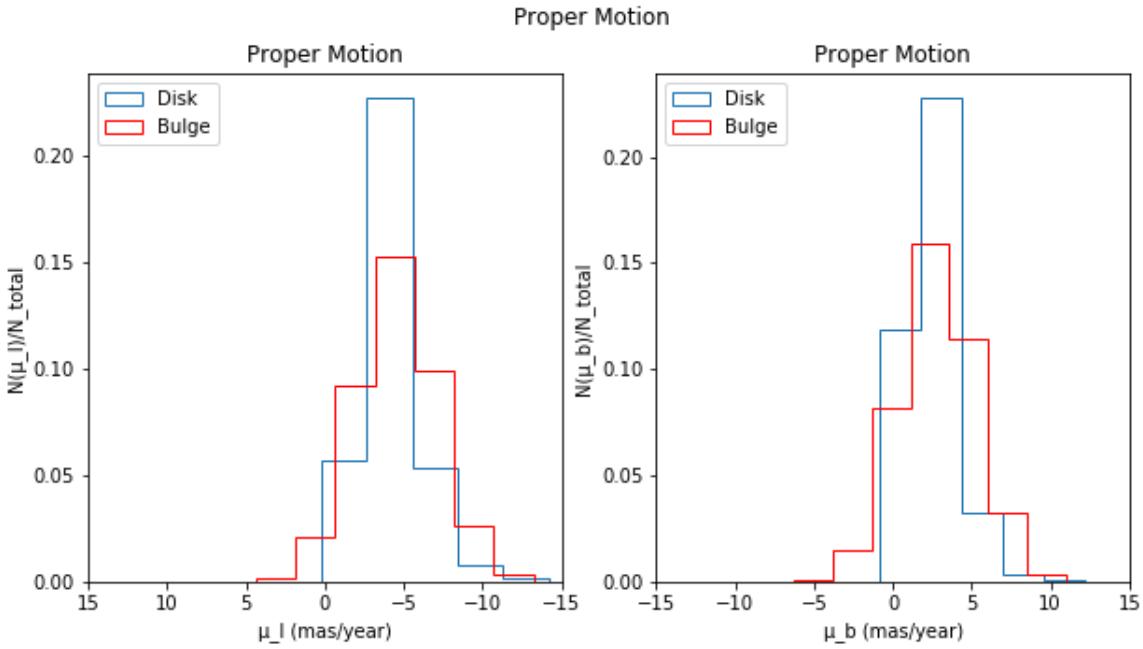

Figure 3.3. A histogram of the proper motion in galactic latitude (b) and galactic longitude (l) from the model output

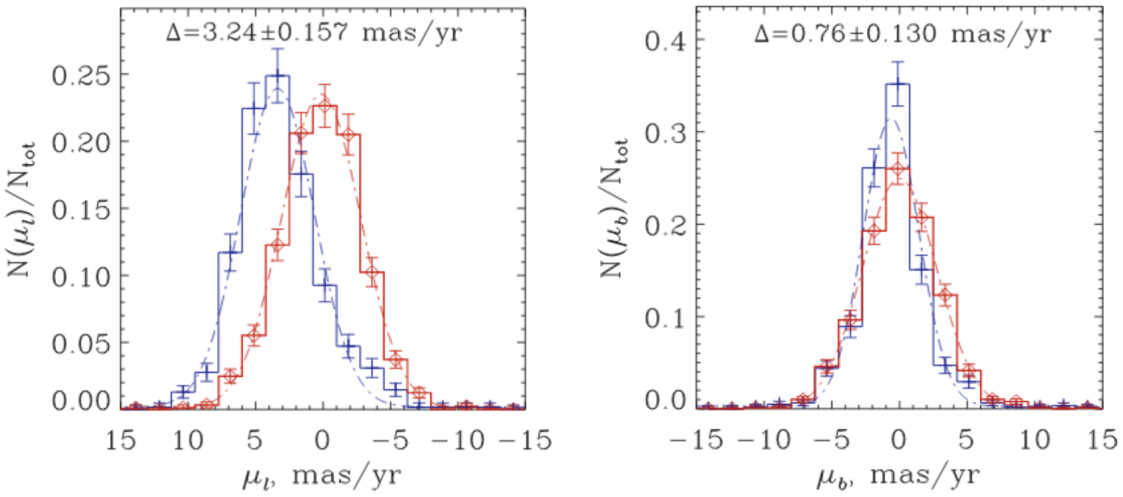

Figure 3.4. A histogram of the proper motion in galactic latitude (b) and galactic longitude (l) from Clarkson et al (2008) [27].

CHAPTER 4. FUTURE AREAS OF IMPROVEMENT

This model has gone through several iterations, each making significant improvements over the last. While this program has come a long way, there are still some aspects that can be improved to ensure that this model is the most accurate, efficient, and modular version available to us.

4.1 Extinction

Further work needs to be done to fully incorporate an extinction model into this program. This is something that is currently being worked on, and would greatly improve efficiency by enabling an accurate and comprehensive output directly from the model, as opposed to requiring the user to apply their own extinction law to model outputs.

4.2 Computational Cost

Computational runtime can always be improved, and this is something that future editions of this model should look into. Currently each star is generated individually, which can take up a lot of time as a star cannot be accepted or rejected until the magnitude is calculated using the stellar isochrones. Because this occurs late in the computational process for each star, it would be more efficient if a group of stars could be generated at once and filtered for those that do not pass the magnitude limit. Additionally, each individual function can likely be optimized further to ensure that it is running in the most efficient manner possible. This is a tedious process, but one that would likely improve the overall runtime of the program. Because large, comprehensive catalogs can take days to run on a personal computer, any reduction in runtime could provide a significant advantage.

4.3 Galactic Bulge

Some initial testing of this model has shown discrepancies in model outputs in the galactic bulge. While this is likely due to an error in the isochrone interpolation, it is worth looking into in more detail to determine the cause of the error. Fixing this would increase our model's effectiveness over other, similar models for the purposes of microlensing detections, as the galactic bulge is the most densely populated region and therefore the best candidate for a high rate of mircolensing events.

4.4 User Input

Currently, user input is allowed through a separate parameter file, which can be edited based on the user's specifications and is read by the program. As one of the primary motivations for designing this new model was for it to be more modular and accessible, it would be beneficial to make as many parameters adjustable by the user as possible. We would also like to be able to incorporate a wider range of magnitude bands and allow for more flexibility in the data that is included in the output.

CHAPTER 5. CONCLUSION

The purpose of this model is to provide a synthesis catalog of stars in the Milky Way Galaxy, meeting parameters as set by the user, to prepare for the microlensing survey on the Nancy Grace Roman Space Telescope. Detecting planets through microlensing will allow us to find many new solar system analogs around other stars, as well as planets in parameter spaces that were previously unexplored. While there are some aspects that will need to be further looked into and improved upon to ensure that it fulfills our needs, this model does a good job of simulating many galactic components and has made important improvements over other available models for our purposes. Overall, this is an ongoing project that will serve as an important aid to the detection of microlensing events in the future.

REFERENCES

[1] B. S. Gaudi, "Microlensing surveys for exoplanets," *Annual Review of Astronomy and Astrophysics*, Jun. 2012.

[2] M. T. Penny, B. S. Gaudi, E. Kerins, S. Mao, A. C. Robin, and S. C. Novati, "Predictions of the wfirst microlensing survey i: Bound planet detection rates," Sep. 2018.

[3] S. Mao, "Introduction to gravitational microlensing," *Proceedings of Science*, Nov. 2008.

[4] L. Cao, S. Mao, D. Nataf, N. J. Rattenbury, and A. Gould, "A new photometric model of the galactic bar using red clump giants a new photometric model of the galactic bar using red clump giants," *Monthly Notices of the Royal Astronomical Society*, Aug. 2013.

[5] J. Bovy, H. W. Leung, J. A. S. Hunt, J. T. Mackereth, D. A. Garcia-Hernandez, and A. Roman-Lopes, "Life in the fast lane: A direct view of the dynamics, formation, and evolution of the milky way's bar," May 2019.

[6] J. Bland-Hawthorn and O. Gerhard, "The galaxy in context: Structural, kinematic & integrated properties," *Annual Review of Astronomy and Astrophysics*, Jan. 2017.

[7] A. J. Deason, V. Belokurov, and J. L. Sanders, "The total stellar halo mass of the milky way," *Royal Astronomical Society*, Dec. 2019.

[8] M. Mayor and D. Queloz, "A jupiter-mass companion to a solar-type star," *Nature*, Nov. 1995.

[9] A. Leger, D. Rouan, J. Schneider, and et al., "Transiting exoplanets from the corot space mission viii. corot-7b: The first super-earth with measured radius," *Astronomy and Astrophysics*, Oct. 2009.

[10] A. Wolszczan and D. A. Frail, "A planetary system around the millisecond pulsar psr1257 + 12," *Nature*, Jan. 1992.

[11] L. R. Doyle, J. A. Carter, D. C. Fabrycky, R. W. Slawson, S. B. Howell, and et al., "Kepler-16: A transiting circumbinary planet," *Science*, Sep. 2011.

[12] M. Gillon, A. H. M. J. Triaud, B.-O. Demory, and et al., "Seven temperate terrestrial planets around the nearby ultracool dwarf star trappist-1," *Nature*, Feb. 2017.

[13] S. Miyazaki, S. A. Johnson, T. Sumi, M. T. Penny, N. Koshimoto, and T. Yamawaki, "Revealing short-period exoplanets and brown dwarfs in the galactic bulge using the microlens-

ing xallarap effect with the nancy grace roman space telescope," *The Astronomical Journal*, Feb. 2021.

[14] S. Mao and B. Paczynski, "Gravitational microlensing by double stars and planetary systems," *Astrophysical Journal*, Jun. 1991.

[15] S. A. Johnson, M. T. Penny, B. S. Gaudi, E. Kerins, N. J. Rattenbury, A. C. Robin, S. C. Novati, and C. B. Henderson, "Predictions of the nancy grace roman space telescope galactic exoplanet survey. ii. free-floating planet detection rates," *The Astronomical Journal*, Sep. 2020.

[16] A. C. Robin, C. Reyle, S. Derriere, and S. Picaud, "A synthetic view on structure and evolution of the milky way," *Astronomy and Astrophysics*, Jul. 2003.

[17] L. Girardi, M. A. T. Groenewegen, E. Hatziminaoglou, and L. da Costa, "Star counts in the galaxy:simulating from very deep to very shallow photometric star counts in the galaxy: Simulating from very deep to very shallow photometric surveys with the trilegal code," *Astronomy and Astrophysics*, Mar. 2005.

[18] S. Pasetto, E. K. Grebel, C. Chiosi, D. Crnojevic, P. Zeidler, G. Busso, L. P. Cassara, L. Piovan, R. Tantalo, and C. Brogliato, "Galmod: A galactic synthesis population model," *The Astrophysical Journal*, Jun. 2018.

[19] S. Sharma, J. Bland-Hawthorn, K. V. Johnston, and J. Binney, "Galaxia: A code to generate a synthetic survey of the milky way," *The Astrophysical Journal*, Mar. 2011.

[20] M. Huston, "Making microlensing predictions with a new population synthesis galactic model," B.S. Thesis, The Ohio State University, Apr. 2018.

[21] P. Kroupa, "On the variation of the initial mass function," Sep. 2000.

[22] O. A. Gonzalez, M. Zoccali, S. Vasquez, V. Hill, M. Rejkuba, E. Valenti, A. Rojas-Arriagada, A. Renzini, C. Babusiaux, D. Minniti, and T. M. Brown, "The giraffe inner bulge survey (gibs) ii. metallicity distributions and alpha element abundances at fixed galactic latitude," *Astronomy and Astrophysics*, Aug. 2015.

[23] M. Steffen, "A simple method for monotonic interpolation in one dimension," *Astronomy and Astrophysics*, Aug. 1990.

[24] J. C. Lagarias, J. A. Reeds, M. H. Wright, and P. E. Wright, "Convergence properties of the nelder-mead simplex method in low dimensions," *Siam Journal on Optimization*, Dec. 1998.

[25] E. Anderson and C. Francis, "Xhip: An extended hipparcos compilation," *Astronomy Letters*, May 2012.

[26] A. Kunder, A. Koch, R. M. Rich, R. de Propris, C. D. Howard, S. A. Stubbs, C. I. Johnson, J. Shen, Y. Wang, A. C. Robin, J. Kormendy, M. Soto, P. Frinchaboy, D. B. Reitzel, H. Zhao, and L. Origlia, "The bulge radial velocity assay (brava). ii. complete sample and data release," *The Astronomical Journal*, Dec. 2011.

[27] W. Clarkson, K. Sahu, J. Anderson, T. E. Smith, T. M. Brown, M. R. Rich, S. Casertano, H. E. Bond, M. Livio, D. Minniti, N. Panagia, A. Renzini, J. Valenti, and M. Zoccali, "Stellar proper motions in the galactic bulge from deep hubble space telescope acs wfc photometry," *The Astrophysical Journal*, Sep. 2008.